Flame stretch and flow patterns induced by Darrieus-Landau instability on a turbulent premixed flame.

G. Troiani[1*], F. Creta[2]

Sustainable Combustion Lab. ENEA C.R. Casaccia, Rome, Italy
Dept. of Mechanical and Aerospace Engineering, University of Rome "La Sapienza", Rome, Italy

Abstract

The effects of Darrieus-Landau (DL) hydrodynamic instability on the hydrodynamic strain exerted on a turbulent flame is analyzed experimentally and numerically (DNS). By varying the equivalence ratio of an air/propane and air/methane mixture the cut-off wave-length is modified and the DL instability induced, the unstable planar flame attaining a corrugated conformation. In this work it is shown that, in the presence of increasing levels of turbulence, the unstable flame front in the neighbourhood of cusps experiences a complex mechanism of compression and extension. The combined effect of incoming flow and flame front self propagation on the flame stretch can be decomposed in three contributions. The first is due to the front propagation velocity, the second is the effect of normal velocity to the front and the last one is the gradient of tangential velocity at the flame front. The different contributions to flame stretch are analyzed and related to the front curvature. Significant differences emerge whether the flame front experiences stable or unstable conditions.

Keywords: Premixed turbulent flames, Bunsen flames, Darrieus-Landau instability, Flame stretch, Flame curvature.

1. Introduction

When the thickness of a premixed flame front can be considered small with respect to the hydrodynamic length scale, the common assumption for flamelets prescribes that such chemically reactive front is conveyed by the turbulent flow field while propagating with a combustion velocity S_L which, in turn, is a complex function not only of the thermo-chemical parameters, but also of the stretch rate the flame undergoes. The result is an alteration of the mean rate at which the fuel is consumed. The rate at which the flame surface varies, the stretch rate, is given by

$$\mathcal{K} = \frac{1}{A}\frac{dA}{dt} , \tag{1}$$

with A the measure of the flame surface. Considering an intrinsic curvilinear reference system attached to the front, with $\mathbf{n}$ the normal vector to the front (pointing towards the products zone), $\boldsymbol{\tau}$ the tangential vector and considering the local flow velocity decomposed into components normal ($v_n\mathbf{n}$) and tangential ($\mathbf{v}_\tau$) to the surface itself, the expression for the flame stretch assumes the form [1]

$$\mathcal{K} = S_L k \underbrace{-v_n k}_{a_n} + \underbrace{\nabla_\tau \cdot \mathbf{v}_\tau}_{a_\tau} , \tag{2}$$

being k the front curvature, $k = -\nabla \cdot \mathbf{n}$. In this form it is easy to give a physical interpretation to each of the term in equation 2. The first term of the equation suggests that an expanding flame, e.g., a spherical expanding flame ($k > 0$), in a quiescent environment is positively stretched, such as a curved flame (convex towards reactants, i.e., $k < 0$) with reactant velocity impinging normally to the front (second term). The last term intuitively recalls expansion when velocity divergence is positive [2]. From this analysis, it emerges that the flame topology and the flow patterns of the embedding flow are decisive factors in flame stretching. In this context, the intrinsic Darrieus-Landau (DL) hydrodynamic instability is crucial and its presence or absence can deeply modify the stretch rate distribution along the flame front.

*Corresponding author
Email address:
guido.troiani@enea.it,francesco.creta@uniroma1.it
(G. Troiani[1*], F. Creta[2])

In a laminar scenario a planar flame can transition to a typical large scale cusp-like structure steadily propagating towards reactants [2]. In the reference system used in equation 2 those cusps have large negative curvature and usually S_L and v_n have opposite sign, yelding the first two terms of equation 2 to counteracting effects upon flame stretch. Moreover, the unstable configuration made of large negative curvature crests sorrounded by smooth troughs with low positive valued curvatures modify the otherwise parallel streamlines of a laminar flow making them focused towards cusp apex. The results into the compression of crests [3].

Turning to turbulent flows, in those cases where hydrodynamic instabilities overwhelm turbulent fluctuations [4], the situation is more complex in that turbulent structures exert a transient positive strain on the flame front rendering it wrinkled. As a consequence, the wrinkled surface of the flame triggers channeling of streamlines causing compression of the crests on one hand and expansion on the other [5].

In a recent study [6] experimental turbulent flame speed measurements in a Bunsen flame at atmospheric pressure were carried out by varying the propane/air mixture ratio so as to act on the cut-off wavelength and thus control the insurgence of DL instability. The classification of observed flames into sub/supercritical regimes, discriminating between stability and instability, is achieved mainly through the characterization of their morphology in terms of flame curvature statistics, whose symmetrical (stable) distribution is altered and skewed by a massive presence of flame front cusp-like structures.

In the present work, several air/propane flames at atmospheric pressure and increasing equivalence ratio and Reynolds number [6] are analyzed in terms of flame stretch and of its dependence on front curvature. Both laminar and turbulent flames are also simulated by a low-Mach DNS. It is found that strain exerted on the flame front ensues a complex mechanism of compression and extension of an unstable turbulent flame front.

2. Results and discussion

Sub/supercritcal regimes are sought in a Bunsen flame in order to analyze their morphology and assess the influence of DL instability on turbulent flame speed. We adopt a Bunsen burner of two different diameters, $D = 18$ mm and $D = 14$ mm at atmospheric pressure, fed with a mixture of air and propane at variable equivalence ratio and at different bulk Reynolds numbers based on nozzle diameter and reactant mass flow rate $\dot{m}$, where $Re = 4\dot{m}/D\mu\pi$. The Reynolds number ranges from a minimum of 1500 up to 10000 and a methane diffusive pilot flame is used to prevent from potential flame blow-off at unstable regimes [7]. For a detailed description of the experiment, measurement techniques and data reduction the reader is addressed to reference [6]. In addition to the present experimental investigation, we perform direct numerical simulations of laminar and turbulent two-dimensional methane/air premixed flames.

2.1. Curvature distribution and total strain rate at low Reynolds number

This section is aimed at discussing relationships between variations of equivalence ratio (of a propane/air mixture burning at atmospheric pressure) and the resulting toplogy of the flame front. Figure 1 exemplifies those changes by representative snapshots of flame images corresponding to increasing equivalence ratios (from left to right, from lean to rich mixtures) at Reynolds number 2500. Following these snapshots

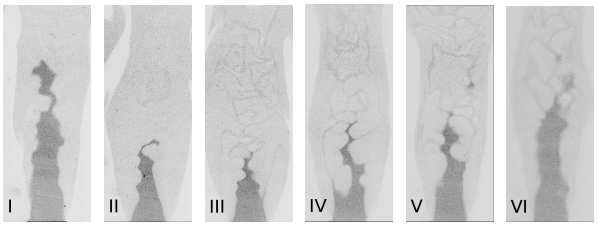

Figure 1: Mie scattering images of C_3H_8/Air flames at varying equivalence ratios (Φ) bulk Reynolds number, (Re), 2500 . Colors have been inverted so that dark zones correspond to reactants. I, $\Phi = 0.7$; II, $\Phi = 0.9$; III, $\Phi = 1.4$; IV, $\Phi = 1.5$; V, $\Phi = 1.6$; VI, $\Phi = 1.7$.

from leaner to richer mixtures a certain increase of cusp-like structures can be observed while finally, at the richest mixtures, the amount of such structures decreases again. This topological transition has been explained with the inception of hydrodynamical instabilities rised by equivalence ratio variations [6].

As the hydrodynamical intabilities are triggered a statistical signature of the front curvature statistics is observed, expressed in terms of the third order moment (skewness) of probability density function (p.d.f.). In the case of statistical presence of cusp-like structures, characterized by large negative values of curvature, the negative tail of probability distribution raises, and the curvature mean value tends to negative values. This implies that the more negative the skeweness value, the stronger the presence of cusp-like structures is. The behavior of skewness depicted in figure 2 exemplifies this trend: values closer to zero highlight more symmetric

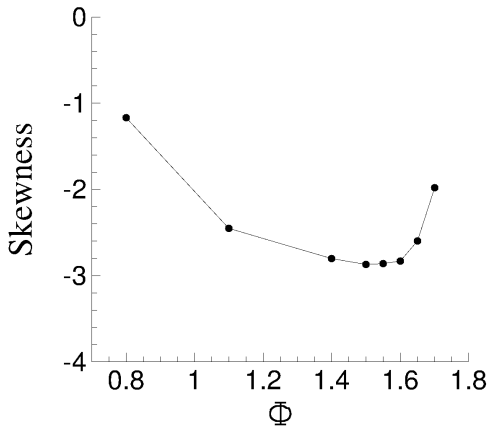

Figure 2: Skewness of flame curvature p.d.f. *vs* equivalence ratio Φ at $Re = 2500$.

distributions attributable to absence of cusp-like structures and subcritical beahavior, whereas negative values indicates higher probability of cusps and supercritical behavior in terms of Darrieus-Landau instability. A concave shape of skewness will underline that at equivalence ratio extrema the system is more prone to stability, hence subcritical, in contrast to mid-values where the supercritical state seems to dominate. In the next section it will be shown how this effect is more evident at lower Reynolds numbers, indicating a lesser degree of influence of turbulent scales.

As combustion involves a strong and mutual interaction between flame front and the fluid-dynamic field, it is equally likely that the velocity field would also experience statistical changes once DL effects are active [8]. With the purpose of scrutinizing the mutual interaction between topology of flame front and flow field, a low Reynolds number flame ($Re = 1500$) is used here.

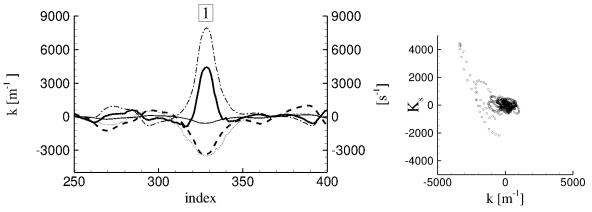

Figure 3: Left,Curvature and strain rate components along the curvilinear abscissa of the front. Lines: thick-dashed line, curvature; dotted line, tangential strain rate $a_\tau = \nabla_\tau \cdot \mathbf{v}_\tau$; dash-dotted line, normal strain rate $a_n = -v_n k$; thick continuous line, total strain rate $a_\tau + a_n$; thin continuous line, curvature contribution to strain rate $S_L k$. Right, Scatter plot curvature *vs* total flame stretch $K_s = a_\tau + a_n$.

Starting from equation 2, flame stretch is decomposed into its three principal components, the first one due to its self-propagation nature (S_L), the second and the third being the normal and tangential components, respectively. Left panel of figure 3 exemplifies the behavior of the individual components of flame stretch. Here the position and amplitude of flame cusp 1 is compared to the amplitude of the components of flame stretch. First of all we note that the term $S_L k$ (thin continuous line) does not effectively contribute to the total amount of stretch. Secondly, the flame front is observed to be subjected to compression due to the tangential strain rate (negative values of dotted line), which in turn comes from the focusing effect of streamlines towards cusp apex [2]. Differences between the current Bunsen case ans a freely propagating planar laminar flame (see [2]) stems from the amplitude of the normal contribution to flame stretch given by the product $-v_n k$ (dash-dotted line). As in the planar case it is clearly positive but its amplitude is large enough to make the total strain (thick continuous line) positive, hence the flame front is expanded. This combined effect of conpression and expansion of flame front close to cusp apex carries its signature in terms of the correlation between curvature and total strain $K_s = a_\tau + a_n$ as can be evinced by the scatter plot displayed in the right panel of figure 3 where the bundle of points at the origin represents the uncorrelated data far from the cusps, while when approaching the cusp apex the flame stretch is strongly and negatively correlated. In order to corroborate the occurrence of such curvature-strain correlation, figure 4 represents another instant of the same flame configuration. Here, four well developed cusps can be observed (labeled $1-4$). A striking anticorrelation between curvature and strain is observable as shown in the inset of the same figure. It can also be noticed that, given the small amplitude of negative curvature, the shoulder portion of cusps, far from the apex, is sligtly compressed. This is also evident in the scatter plot panel with a certain degree of positive correlation. Sumarizing, scatter plots are characterized by a positive correlation at small negative amplitudes of curvature and strain (cusp shoulder) and an anticorrelation at cusp apex when both curvature and strain are large.

According to the classification grounded on skewness data plotted in figure 2 the same Reynolds number flame at leaner mixture of $\Phi = 0.8$ should lack cusp-like structures. The result is that curvature and total flame stretch are not correlated. Figure 5 encompasses joint p.d.f. of a large number of flame samples at Reynolds number of 1500 and equivalence ratio Φ 0.8 and 1.5, which are classified as subcritical and supercritical, respectively.

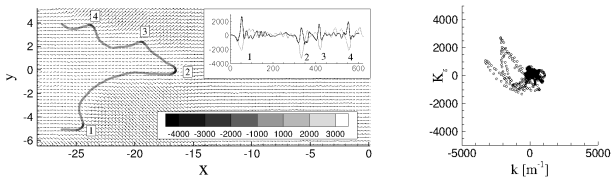

Figure 4: Left, snapshot at Reynolds number 1500 and equivalence ratio $\phi = 1.5$. In the inset, curvature (dashed line) and total flame stretch (bold line), see caption of figure 3 for further details. Right, Scatter plot curvature *vs* total flame stretch $K_s = a_\tau + a_n$.

Subcritical flames are characterized by a symmetrical distribution of joint p.d.f. data in contrast to the presence of a preferential alignment of large negative curvatures with large positive total strain when the supercritical state is present.

2.2. *Effect of increasing turbulence level*

As turbulence intensity increases, a less pronounced influence of hydrodynamic instability is expected on the flame front dynamics which is now strongly perturbed by turbulent velocity fluctuations [4, 6, 8]. A condition for this to occur calls for the turbulence time scales to be smaller than DL growth rates, effectively keeping the instabilities from developing. In particular, the existence of a DL-enhanced turbulent propagation regime is subject to the condition that at a flame perturbation wavenumber k its linear growth rate ω, given by the dispersion relation, be greater than the characteristic eddy frequency $\omega_{\text{turb}} = 2\pi/\tau_{\text{turb}}$ where τ_{turb} is the eddy turnover time estimated as the ratio of turbulent kinetic

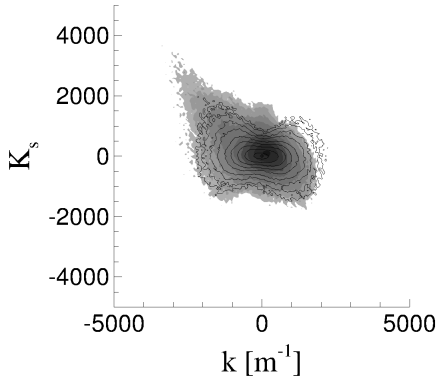

Figure 5: Joint pdf curvature *vs* total flame stretch $K_s = a_\tau + a_n$ of flames at Reynolds number 1500 and differrent equivalence ratios: contour lines, $\Phi = 0.8$ (subcritical); gray tones, $\Phi = 1.5$ (supercritical)

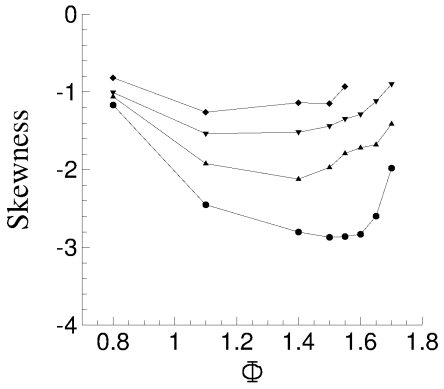

Figure 6: Third moment of curvature p.d.f. *vs* equivalence ratio at increasing Reynolds number. Symbols: Circles, $Re = 2500$; delta, $Re = 5000$; gradient, $Re = 7000$; diamonds, $Re = 10000$.

energy to mean dissipation rate [4]. Hence, when hydrodynamic instabilities are progressively overpowered by increasing levels of turbulence, not only the flame front toplogy but also its mutual interaction with the velocity field should change. To asses this statement, a number of experiments with turbulent velocity fluctuations progressively increased are carried out. In particular, for every equivalence ratio that spans between 0.8 and 1.7, four Reynolds numbers are analyzed, namely $Re = 2500, 5000, 7000, 10000$. As Reynolds numbers are raised, a qualitative visual inspection of flame snapshots seeking for cusp-like structures resulted meaningless due to the high presence of fine wrinkled front structures induced by turbulence. A statistical analysis of flame front curvatures is however performed and results shown in figure 6. When the Reynolds number is increased the concavity of skewness distribution is reduced and values progressively tends towards zero, which underlines a symmetric shape of p.d.f. distribution. This particular trend can be read in terms of the overpowering of hydrodynamic instabilities by the incresing level of turbulence.

Same tendency is retrieved in joint p.d.f. of total strain and curvature shown in figures 7. Following the increase of equivalence ratio in the case at Reynolds 2500 (see figure 5) inception of hydrodynamic instability can be perceived by noticing the increased negative correlation between total strain and curvature. As in previous skewness analysis, leaner and richer mixtures can be considered subcritical whereas at near stoichiometric values the flame is subject to DL instability. As Reynolds number is increased such correlation is mitigated and the amplitude of total strain increases noticeably and its distribution homogenized with high

levels of fluctuations in all directions. This different behavior is striking at Reynolds 10000 indicating that a turbulence driven regime is reached.

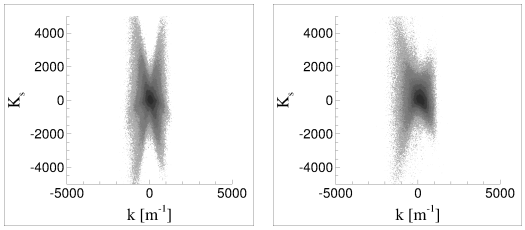

(a) Re = 10000 Φ = 0.8 (b) Re = 10000 Φ = 1.1

(c) Re = 10000 Φ = 1.4 (d) Re = 10000 Φ = 1.55

Figure 7: Joint p.d.f. front curvature *vs* total strain.

3. CFD of Bunsen and planar Flames

Following our previous study [6], in addition to the present experimental investigation, we perform direct numerical simulations of laminar and turbulent two-dimensional methane/air premixed flames. We adopt a numerical scheme based on the unfiltered, low-Mach number, reactive Navier-Stokes equations with detailed chemical kinetics. Full details of the scheme can be found in [9, 10] while the kinetic mechanism is a CSP-simplified [11] version of the Gri1.2 mechanism, comprising 16 species and 57 reactions. Grid resolution is kept at 45μm to ensure a minimum of 10 grid points within the flame thickness when this is defined using the temperature profile.

An initial simulation is performed to study a mildly perturbed, freely propagating flame in a quiescent mixture and spanwise periodic conditions. A complex fluid structure thus emerges, due entirely to the DL instability, which induces both normal and tangential hydrodynamic straining, ultimately exerting compressive and expansive effects on the flame.

Taking the T = 350K isocontour as a representative boundary between the fresh mixture and the preheat zone, we can extract normal and tangential fluid velocity components at such boundary and estimate normal and tangential components of the total hydrodynamic strain

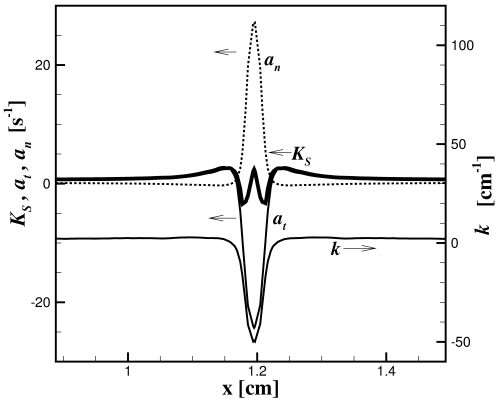

Figure 8: Straining pattern for a DL cusp-like flame.

$K_S = a_n + a_t$. Figure 8 displays both flame curvature κ as well as overall strain and its components, extracted for the central cusp-like structure of the laminar flame. What emerges is a straining pattern in which normal and tangential straining systematically counteract each other. In particular, normal straining is negligible everywhere except at the tip of the cusp where curvature is negative and where a_n attains a positive value. On the other hand, tangential straining a_t is dominating on the troughs of the cusp where it attains small positive values, while on the cusp sides and on the crest it attains negative values. Thus a complex straining picture emerges according to which the flame is only mildly extended ($K_S > 0$) at the troughs while it is compressed ($K_S < 0$) on the cusp sides. At the cusp tip, however, due to a dominating effect of the normal component, the flame is subject to a mildly positive strain rate. An

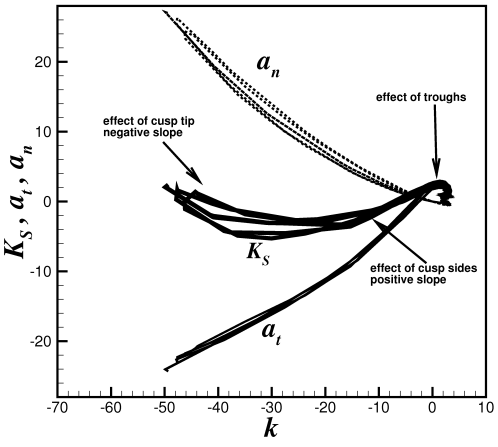

Figure 9: Correlation between overall strain rate and its components to flame curvature.

effective visualization of these phenomena is obtained in Fig 9 where the correlation of normal and tangential straining components to flame curvature is examined. As mentioned, we can clearly observe the negative correlation of a_n to curvature and the opposite positive correlation of a_t and their effect on the correlation of the overall strain rate K_S on curvature. We observe that the positive correlation due to tangential strain rate is dominating at the troughs and at the cusp sides where curvature is either mildly positive or moderately negative, while the correlation due to normal strain rate becomes dominating at the cusp tip where highly negative values of curvature are experienced.

The above correlation patterns between strain and curvature in the presence of DL instability and valid in laminar conditions seems to have a universal character and be rather independent of the choice of the representative temperature isocontour, provided this is taken on the unburned side of the flame. A very similar pattern was also discussed in [2] using a hybrid level-set Navier-Stokes technique.

The question arises as to whether similar correlation patterns exist in a turbulent scenario. For this reason, additional cfd simulations are performed, this time using a Bunsen flame setting so that a premixed front can be stabilized within an incident turbulent flow of incoming fresh gases. The simulation is identical to that described in [6] and the reader is address to such reference for further details. The same technique used for the laminar case is adopted in the turbulent scenario to extract strain rate and curvature information. Figure 10

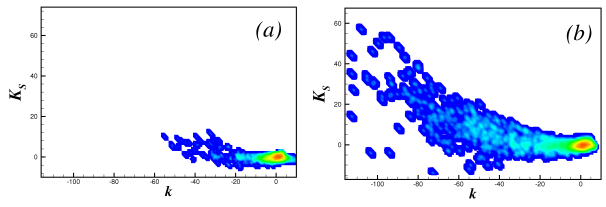

Figure 10: Joint p.d.f. of flame curvature and strain rate for a two-dimensional Bunsen flame in (a) stable (b) unstable conditions.

displays the correlation for a turbulent Bunsen flame in stable and unstable conditions, i.e. in such conditions that DL induces cusp-like structure are respectively absent or present. It is evident that in unstable conditions a similar scenario observed with the laminar flame in Fig. 8 arises with cusp tips being responsible for the negative correlation at highly negative curvatures and a mildly positive correlation due to troughs and cusp sides. Under stable conditions the above correlation patterns seems to be far less evident if not absent, with a surviving small negative correlation possibly due to Huygens effect giving rise to temporary cusping. At higher values of turbulence intensity, we expect this correlation pattern to dissipate as the DL-induced structures will be increasingly overshadowed by turbulent wrinkling.

4. Final comments

In the present work, several air/propane and air/methane flames at increasing equivalence ratio and Reynolds number have been analyzed in terms of flame stretch and of its dependence on front curvature. It is found that strain exerted on the flame front causes a complex mechanism of compression and extension of an unstable turbulent flame front. The competition between turbulence and hydrodynamic instability timescales is also highlighted, revealing that the influence of DL instabilities is concealed at increasing level of turbulence intensity.

References

[1] M. Matalon, C. Cui, J. Bechtold, J. Fluid Mech. 487 (2003) 179–210.

[2] F. Creta, M. Matalon, Proc. Comb. Inst. 3 (2011) 1087–1094.

[3] K. Law Chung, Combustion physics, Cambridge University Press, 2006.

[4] S. Chaudhuri, V. Akkerman, C. Law, Phys. Rev. E 84 (2011).

[5] A. M. Steinberg, J. F. Driscoll, S. L. Ceccio, Proceedings of the Combustion Institute 32 (2009) 1713–1721.

[6] G. Troiani, F. Creta, M. Matalon, Proceedings of the Combustion Institute (2014).

[7] G. Troiani, Combust. Flame 156 (2009) 539–542.

[8] J. Yuan, Y. Ju, C. K. Law, Physics of Fluids (1994-present) 18 (2006) 104105.

[9] O. Knio, H. Najm, P. Wyckoff, J. Comput. Phys. 154 (1999) 428–467.

[10] H. Najm, P. Wyckoff, O. Knio, J. Comput. Phys. 143 (1998) 381–402.

[11] M. Valorani, F. Creta, D. Goussis, J. Lee, H. Najm, Combustion and Flame 146 (2006) 29–51.